Rock physics modeling using machine learning

Lian Jiang and John P. Castagna, Department of Earth and Atmospheric Sciences, University of Houston;*
Brian Russell, CGG; Pablo Guillen, Hewlett Packard Enterprise Data Science Institute, University of Houston

Summary

The assumptions made in rock physics theories introduce many uncertainties into conventional rock physics modeling (RPM), which makes it difficult to implement accurate quantitative seismic interpretation workflows. We propose using machine learning algorithms to address this issue. First, we build a theoretical rock physics model using a conventional RPM workflow. We use Hertz-Mindlin grain contact theory to estimate the moduli of rock frame with optimized model parameters. We then use this rock physics model to create synthetic well logs by perturbing the rock properties, such as lithology and porosity. Next, we use the synthetic wells to test the efficacy of three common machine learning algorithms: support vector regression (SVR), random forest (RF), and the multi-layer perceptron (MLP). Finally, we predict *P*- and *S*-wave velocity by utilizing both the machine learning algorithms and the rock physics model on measured data from wells. Our proposed method achieves a better result than conventional rock physics modeling, with the average R^2 score (coefficient of determination) increasing by 25.8% on *P*-wave prediction and 64.0% on *S*-wave prediction.

Introduction

The main task of RPM is to estimate the elastic parameters of rocks with known mineral composition, porosity, and pore geometry, etc. (e.g. Biot (1941), Gassmann (1951), Walsh (1965), Kuster and Toksoz (1974), Brown and Korringa (1975), Berryman (1980), Castagna et al. (1985), Han (1986) and Greenberg and Castagna (1992)). In general, we can group these rock physics models into three classes: theoretical, empirical, and heuristic (Avseth et al., 2005). Many of the rock physics models achieve good results in the estimation of elastic parameters such as *P*- and *S*-wave velocity, but they all contain many underlying assumptions. For example, the inclusion theoretical models assume the pores are ellipsoidal or some other regular shape (Eshelby, 1957; Walsh, 1965; Kuster and Toksoz, 1974; Berryman, 1980; Jakobsen et al. 2003). However, the pores in real rocks can be any irregular shape. The heuristic models make fewer theoretical assumptions than theoretical models, but still suffer from not being able to capture the underlying complexity of many rocks. Empirical rock physics models, (e.g. Castagna et al. (1985) and Han (1986)), make even fewer assumptions than theoretical and heuristic models, but still have limitations when applied to real world situations, as they are derived from only a subset of real cases. For instance, we can only use the Greenberger and Castagna equations (1992) to predict *S*-wave velocity for brine sands.

We investigate how to use machine/deep learning algorithms to build a rock physics relationship between mineral/lithology composition, porosity, water saturation, pressure, density, and *P*- and *S*-wave velocity. To evaluate the performance of our proposed method, we will compare the prediction results with conventional RPM approaches.

Conventional rock physics modeling

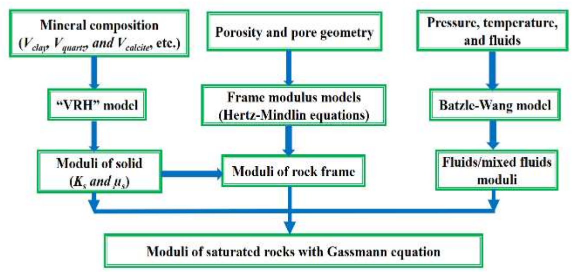

Figure 1: Workflow for conventional theoretical rock physics modeling.

Figure 1 is the workflow of a conventional theoretical rock physics modeling method. We use the Voigt-Ruess-Hill (VRH) average equation to calculate the bulk and shear moduli of solid rock matrix and the Batzle-Wang (BW) model to calculate the fluids/mixed fluids bulk modulus. However, appropriately estimating the moduli of the rock frame is one of the biggest challenges in this work. Many researchers have studied this issue (e.g. Kuster and Toksoz (1974)). We choose the Hertz-Mindlin (HM) grain-contact theory (Ruiz, 2009; Grana, 2016) to build our model. The equations in this theory are:

$$K_{fr} = \left(\frac{\phi/\phi_c}{K_{HM}+4/3\mu_s} + \frac{1-\phi/\phi_c}{K_s+4/3\mu_s}\right)^{-1} - \frac{4}{3}\mu_s, \qquad (1)$$

and

$$\mu_{fr} = \left(\frac{\phi/\phi_c}{\mu_{HM}+\xi} + \frac{1-\phi/\phi_c}{\mu_s+\xi}\right)^{-1} - \xi, \qquad (2)$$

where

$$\xi = \frac{1}{6}\mu_s \frac{9K_s+8\mu_s}{K_s+2\mu_s}, \qquad (3)$$

where K_{fr} is frame bulk modulus, μ_{fr} is shear modulus, ϕ is porosity, μ_s is solid shear modulus, K_s is solid bulk modulus, ϕ_c is critical porosity, K_{HM} is frame bulk modulus at critical porosity and μ_{HM} is the corresponding frame shear modulus, which are defined as

10.1190/segam2020-3427097.1

$$K_{HM} = \left(\frac{C(1-\phi_c)\mu_s}{3\pi(1-\sigma_s)}\left[\frac{3\pi}{2}\frac{(1-\sigma_s)}{(1-\phi_c)C}\frac{P_d}{\mu_s}\right]^{1/3}, \quad (4)$$

and

$$\mu_{HM} = \left(\frac{3K_{HM}}{5}\frac{[2-\sigma_s+3\gamma(1-\sigma_s)]}{(2-\phi_c)}, \quad (5)$$

where C is coordination number, γ is friction coefficient, and σ_s is solid Poisson's ratio. The solid properties are determined from logged lithology, nominal mineral composition for each lithology, handbook values of mineral elasticity, and VRH averaging.

To use these equations (1-5) to estimate the bulk and shear moduli of the rock frame, we need to know the model parameters (C, γ, and ϕ_c). Although we do not know their exact values, we know their possible range. For instance, the critical porosity is approximately between 30% and 45%. Therefore, we need to estimate the value of the model parameters in a particular scenario. The procedure we use to achieve this goal is:

1) Calculate K_{dry} and μ_{dry} with well log data (including S_w), using the Gassmann equation;
2) Set reasonable ranges for the three HM model parameters according to their physical meaning: C, γ, and ϕ_c, with discrete values within each range;
3) For each combination of HM parameters in step 2), calculate K_{dry} and μ_{dry} throughout the wells using the HM equations;
4) Separate the K_{dry} and μ_{dry} from step 1) and 3) into shale, sand, and carbonates based on their respective volume percentage (from logs);
5) For each lithology, calculate the combined R^2 score of the K_{dry} and μ_{dry} calculated from the Gassmann equation and from the HM equations;
6) Search all model parameter combinations for the optimal model parameters set that achieves the highest total R^2 score for each lithology.

Figure 2 displays the result calculated using this optimization procedure. It shows that the model log curves (red) match the bulk and shear moduli (black) calculated using the Gassmann equation very well (see the detailed optimal model parameters in Table 1), with the R^2 score of 0.70 for the estimation of frame bulk modulus and 0.62 for the estimation of frame shear modulus, respectively.

	ϕ_c	C	γ
Shale	0.33	2.0	0.56
Sand	0.42	6.7	0.01
Carbonates	0.40	6.7	0.64

Table 1: The optimized model parameters for each lithology.

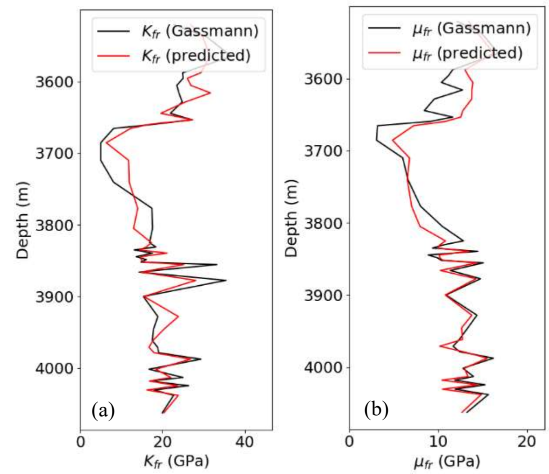

Figure 2: Predictions of the bulk and shear moduli of rock frame using the HM equations. The black curve is the bulk and shear frame moduli calculated using well log data and the Gassmann equation. The red curve is the bulk and shear frame moduli calculated using the well log data and the HM equations with optimized model parameters. (a) Bulk frame modulus; (b) Shear frame modulus.

Machine learning methods

Machine learning explores the study and construction of algorithms that can learn from and make predictions on data. Often it is difficult to predict which algorithm would perform the best, and the performance of data models strongly depends on the features of the provided data set. In order to reach the maximum performance, it is necessary to train each model multiple times with different hyper-parameters options to reach the maximum accuracy and stability in predictions.

We tested three different machine learning algorithms: 1) support vector regression (SVR); 2) random forest (RF); and 3) multi-layer perceptron (MLP). SVR (Cortes and Vapnik, 1995; Drucker et al., 1996) and RF are two of the most common conventional machine learning algorithms.

The MLP (Goodfellow et al., 2016) is a deep artificial neural network (DNN), i.e. it is composed of more than one perceptron. The MLPs are composed of an input layer to receive the signal, an output layer that makes a decision or prediction about the input, and in between those two, an arbitrary number of hidden layers that are the true computational engine of the MLP. Through proper training, the network can learn how to optimally represent inputs as features at different scales or resolutions and combine them into higher-order feature representations relating these representations to output variables and therefore learning how to make predictions. In order to achieve high accuracy in prediction, two dependent problems have to be addressed when solving problems with the MLPs: network architecture

10.1190/segam2020-3427097.1

and training routine. Defining network architectures involves setting fine-grained details such as activation functions and the types of layers as well as the overall architecture of the network. Defining training routines involves setting the learning rules, the loss functions, regularization techniques, and hyper-parameters optimization.

Synthetic data test

In order to test the efficacy of the machine learning algorithms in RPM, we first created synthetic wells using the conventional rock physics model described in figure 1. We created 30 synthetic wells with enough variations so that each synthetic well has different lithology, porosity, water saturation and differential pressure, as well as *P*- and *S*-wave velocity and density.

We use 29 wells of these 30 wells to train and test the machine learning algorithms, and one well as a blind data to validate the performance. In the training process, approximately 80% of the 29 wells is used for training, and approximately 20% is used as the testing set. Figure 3 is the *P*-wave velocity predicted from the SVR, RF, and MLP algorithms, respectively. The average accuracy is above 98% for all of them, with RF achieving the highest accuracy of 99.8%. In other words, the machine learning algorithms work very well on a synthetic data set, which gives us confidence to apply them to field well data.

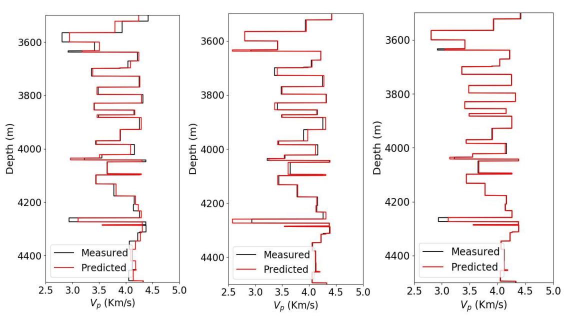

Figure 3: The *P*-wave velocity predicted using the SVR (left), RF (middle), and MLP (right) algorithms. The accuracy is 98.5%, 99.8%, and 99.2% for them, respectively.

Real data test

The well data we use is from Volve oil field, located in the central part of North Sea. Four wells in the field have complete well logging suites. We cleaned the data before using them in our calculation, since any noise in the logs will introduce bias in the training of a neural network.

To make a prediction on each well, we use the other three wells to train the machine learning algorithms, and then use the trained model to make the prediction on this well. We predicted *P*-wave velocity using the theoretical rock physics model built with the workflow described in Figure 1 and the optimized model parameters from Table 1. Figure 4 displays the *P*-wave velocity predictions for the four different wells. We calculate the average prediction accuracy and R^2 score using these four wells. The average prediction accuracy is approximately 93.9%, but the average R^2 score only about 0.67. We use both the prediction accuracy and R^2 score to evaluate our result, because the R^2 can evaluate the prediction variation better than the average prediction accuracy.

We also predicted *P*-wave velocity using the three machine learning algorithms introduced previously. Figure 5 shows the prediction results from the MLP. As we can see, the results look much better than that of conventional RPM. We have improved both the accuracy and R^2 score for each well, with an average prediction accuracy of 95.3% and average R^2 score of 0.79. In particular, the improvement in the R^2 score is encouraging.

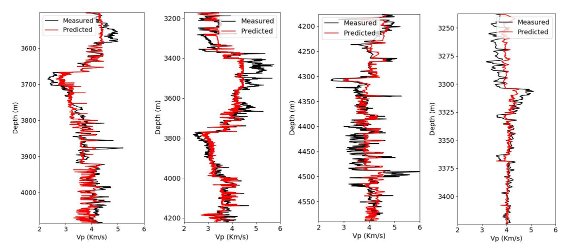

Figure 4: The V_p predictions from the conventional RPM for wells 19A, BT2, SR, and F1-B (from left to right). The black curve is measured V_p and the red curve is the predicted V_p.

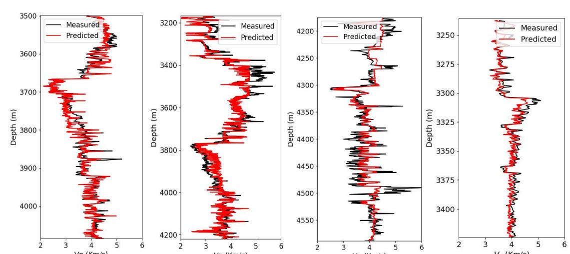

Figure 5: The V_p predictions using the MLP for wells 19A, BT2, SR, and F1-B (from left to right). The black curve is measured V_p and the red curve is the predicted V_p.

We made the similar predictions and comparison on *S*-wave velocity. Figure 6 shows the comparison of the *S*-wave velocity predictions between the MLP and conventional RPM for two different wells. We observe an obvious improvement from the conventional RPM to the MLP results, with an average R^2 score increasing from 0.54 to 0.82, although the predictions are not as good as the V_p predictions.

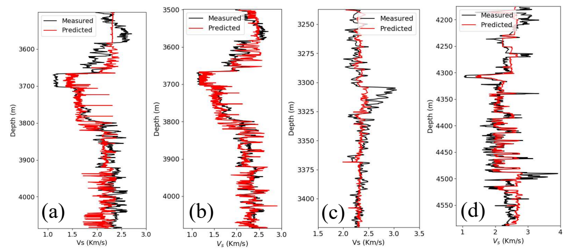

Figure 6: The V_s predictions from the conventional RPM and MLP for wells 19A and F1-B. (a) The prediction result from well 19A using conventional RPM, with accuracy = 86.9% and R^2 score = 0.45. (b) The prediction result from well 19A using the MLP, with accuracy = 92.7% and R^2 score = 0.75. (c) The prediction result from well F1-B using conventional RPM, with accuracy = 95.6% and R^2 score = 0.17. (d) The prediction result from well F1-B using the MLP, with accuracy = 96.5% and R^2 score = 0.62.

Table 2 is the summary for the *P*-wave predictions of all four wells using different methods. In general, we can observe an obvious improvement of the prediction results from the conventional RPM to the machine learning methods. Different machine learning algorithms behave differently for different wells, although the difference between them is not large. The average prediction accuracy for all the wells increases by 2.0%, but the average R^2 score increases by 25.8%, with the lowest increase of 8.5% to the highest increase of 52.1%.

Well name	Metrics	RPM	SVM	RF	MLP
19A	Accuracy	93.9%	95.5%	94.2%	95.7%
	R^2 score	0.82	0.88	0.82	0.89
BT2	Accuracy	93.6%	95.0%	92.6%	94.0%
	R^2 score	0.81	0.89	0.77	0.86
SR	Accuracy	92.8%	93.2%	95.5%	94.8%
	R^2 score	0.55	0.60	0.73	0.67
F1-B	Accuracy	95.2%	91.6%	95.9%	96.5%
	R^2 score	0.48	-0.35	0.44	0.73

Table 2: Summary for the *P*-wave predictions of all four wells using different methods.

Table 3 is the summary for the *S*-wave predictions of all four wells using different methods. We observe an obvious improvement in the *S*-wave prediction results from the conventional RPM to machine learning methods. The average prediction accuracy for all the wells increases by 2.8%, and the average R^2 score increases by 64.0%, with the lowest increase of 6.6% to the highest increase of 114%.

Well name	Metrics	RPM	SVM	RF	MLP
19A	Accuracy	90.5%	94.3%	90.8%	93.9%
	R^2 score	0.71	0.87	0.69	0.87
BT2	Accuracy	91.2%	93.1%	87.8%	92.5%
	R^2 score	0.76	0.81	0.50	0.79
SR	Accuracy	88.5%	90.9%	91.2%	91.5%
	R^2 score	0.30	0.57	0.49	0.64
F1-B	Accuracy	96.2%	95.6%	96.4%	97.6%
	R^2 score	0.36	0.41	0.49	0.77

Table 3: Summary for the *S*-wave predictions of all 4 wells using different methods.

Conclusions

We build a conventional theoretical rock physics model and test how well machine learning algorithms can simulate the rock physics relationship. The synthetic data test reveals that the machine learning algorithms we use in this approach predict *P*-wave velocity very well, with the average prediction accuracy of 99.2%. We also find that different machine learning algorithms perform differently on different wells. Comparison of the predictions of *P*- and *S*-wave velocity on real well data between the conventional rock physics modeling and the machine learning algorithms indicates that the machine learning algorithms achieve a better result than conventional rock physics modeling, with the average R^2 score increasing by 25.8% for *P*-wave predictions and 64.0% for *S*-wave predictions, respectively.

Acknowledgments

The authors would like to thank the research computing data core center from University of Houston for providing computing resources and Equinor for providing the well log and seismic data in this research. We also want to thank Dr. Yi Wang and Dr. Tom Smith for their very useful suggestions and discussion. At last, we want to give many special thanks to Dr. Thomsen for his genuine suggestions and help in this work.

REFERENCES

Avseth, P., T. Mukerji, and G. Mavko, 2005, Quantitative seismic interpretation: Applying rock physics tools to reduce interpretation risk: Cambridge University Press.

Biot, M. A., 1941, General theory of three-dimensional consolidation: Journal Applied Physics, **12**, 155–164, doi: https://doi.org/10.1063/1.1712886.

Brown, R. J. S., and J. Korringa, 1975, On the dependence of the elastic properties of a porous rock on the compressibility of the pore fluid: Geophysics, **40**, 608–616, doi: https://doi.org/10.1190/1.1440551.

Berryman, J. G., 1980, Long-wavelength propagation in composite elastic media: Journal of Acoustic Society of America, **68**, 1809–1819, doi: https://doi.org/10.1121/1.385171.

Castagna, J. P., M. L. Batzle, and R. L. Eastwood, 1985, Relationships between compressional wave and shear wave velocities in clastic silicate rocks: Geophysics, **50**, 571–581, doi: https://doi.org/10.1190/1.1441933.

Cortes, C., and V. Vapnik, 1995, Support-vector networks: Machine Learning, **20**, 273–297.

Drucker, H., C. J. C. Burges, L. Kaufman, A. Smola, and V. Vapnik, 1996, Support vector regression machines: Advances in Neural Information Processing Systems, **9**, 155–161.

Eshelby, J. D., 1957, The determination of the elastic field of an ellipsoidal inclusion, and related problems: Proceedings of the Royal Society of London, 376–396.

Gassmann, F., 1951, Uber die Elastizitat poroser Medien: Vierteljahrsschrift der Naturforschenden Gesellschaft in Zurich, **96**, 1–23.

Greenberg, M. L., and J. P. Castagna, 1992, Shear-wave estimation in porous rocks: Theoretical formulation, preliminary verification and applications: Geophysical Prospecting, **40**, 195–209, doi: https://doi.org/10.1111/j.1365-2478.1992.tb00371.x.

Grana, D., 2016, Bayesian linearized rock-physics inversion: Geophysics, **81**, no. 6, D625–D641, doi: https://doi.org/10.1190/geo2016-0161.1.

Goodfellow, I., Y. Bengio, and A. Courville, 2016, Deep learning: MIT Press.

Han, D., 1986, Effects of porosity and clay content on acoustic properties of sandstones and unconsolidated sediments: Ph.D. dissertation, Stanford University.

Jakobsen, M., J. Hudson, and T. Johansen, 2003, T-matrix approach to shale acoustics: Geophysics Journal International, **154**, 533–558, doi: https://doi.org/10.1046/j.1365-246X.2003.01977.x.

Kuster, G. T., and M. N. Toksoz, 1974, Velocity and attenuation of seismic waves in two-phase media — Part 1: Theoretical formulations: Geophysics, **39**, 587–606, doi: https://doi.org/10.1190/1.1440450.

Ruiz, F. J., 2009, Porous grain model and equivalent elastic medium approach for predicting effective elastic properties of sedimentary rocks: Ph.D. dissertation, Stanford University.

Walsh, J. B., 1965, The effect of cracks on the compressibility of rock: Journal of Geophysical Research: **70**, 381–389, doi: https://doi.org/10.1029/JZ070i002p00381.